AMERICAN SOCIETY FOR MICROBIOLOGY | mBio®

RESEARCH ARTICLE
Applied and Environmental Science

Photoferrotrophs Produce a PioAB Electron Conduit for Extracellular Electron Uptake

Dinesh Gupta,[a] Molly C. Sutherland,[a] Karthikeyan Rengasamy,[a] J. Mark Meacham,[b,c] Robert G. Kranz,[a] Arpita Bose[a]

[a]Department of Biology, Washington University in St. Louis, St. Louis, Missouri, USA
[b]Department of Mechanical Engineering and Materials Science, Washington University in St. Louis, St. Louis, Missouri, USA
[c]Institute of Materials Science and Engineering, Washington University in St. Louis, St. Louis, Missouri, USA

ABSTRACT Photoferrotrophy is a form of anoxygenic photosynthesis whereby bacteria utilize soluble or insoluble forms of ferrous iron as an electron donor to fix carbon dioxide using light energy. They can also use poised electrodes as their electron donor via phototrophic extracellular electron uptake (phototrophic EEU). The electron uptake mechanisms underlying these processes are not well understood. Using *Rhodopseudomonas palustris* TIE-1 as a model, we show that a single periplasmic decaheme cytochrome *c*, PioA, and an outer membrane porin, PioB, form a complex allowing extracellular electron uptake across the outer membrane from both soluble iron and poised electrodes. We observe that PioA undergoes postsecretory proteolysis of its N terminus to produce a shorter heme-attached PioA (holo-$PioA_C$, where $PioA_C$ represents the C terminus of PioA), which can exist both freely in the periplasm and in a complex with PioB. The extended N-terminal peptide controls heme attachment, and its processing is required to produce wild-type levels of holo-$PioA_C$ and holo-$PioA_C$B complex. It is also conserved in PioA homologs from other phototrophs. The presence of PioAB in these organisms correlate with their ability to perform photoferrotrophy and phototrophic EEU.

IMPORTANCE Some anoxygenic phototrophs use soluble iron, insoluble iron minerals (such as rust), or their proxies (poised electrodes) as electron donors for photosynthesis. However, the underlying electron uptake mechanisms are not well established. Here, we show that these phototrophs use a protein complex made of an outer membrane porin and a periplasmic decaheme cytochrome (electron transfer protein) to harvest electrons from both soluble iron and poised electrodes. This complex has two unique characteristics: (i) it lacks an extracellular cytochrome *c*, and (ii) the periplasmic decaheme cytochrome *c* undergoes proteolytic cleavage to produce a functional electron transfer protein. These characteristics are conserved in phototrophs harboring homologous proteins.

KEYWORDS photoferrotrophy, phototrophic EEU, *Rhodopseudomonas palustris* TIE-1, decaheme cytochrome *c*, Fe(II)-oxidation

Several anoxygenic (nonoxygen evolving) phototrophs can grow by coupling oxidation of ferrous iron to carbon dioxide (CO_2) fixation using the energy of light, a process called photoferrotrophy (1). Photoferrotrophy plays an important role in biogeochemical cycling of iron and impacts microbial ecology in marine and freshwater ecosystems (2–4). A phylogenetically diverse group of bacteria carry out this process in natural environments (5). Photoferrotrophs use both soluble ferrous iron [Fe(II)] and insoluble mixed-valence iron minerals as electron donors (6, 7). Photoferrotrophy is considered to be one of the most ancient types of photosynthesis and may represent a transition state between anoxygenic and modern oxygenic photosynthesis (8). In addition, photoferrotrophy is suggested as a primary metabolism responsible for early

Citation Gupta D, Sutherland MC, Rengasamy K, Meacham JM, Kranz RG, Bose A. 2019. Photoferrotrophs produce a PioAB electron conduit for extracellular electron uptake. mBio 10:e02668-19. https://doi.org/10.1128/mBio.02668-19.

Editor Arash Komeili, University of California, Berkeley

Address correspondence to Arpita Bose, abose@wustl.edu.

This article is a direct contribution from Robert G. Kranz, a Fellow of the American Academy of Microbiology, who arranged for and secured reviews by Gemma Reguera, Michigan State University, and Julia Maresca, University of Delaware.

Received 7 October 2019
Accepted 10 October 2019
Published 5 November 2019

marine productivity (9) and a potential process responsible for the deposition of the archean banded iron formations (BIFs) (1, 10–13). Photoferrotrophs can also use electrons from a poised electrode to fix CO_2 with light, a process called phototrophic extracellular electron uptake (EEU) (14, 15). Microbes capable of phototrophic EEU are good candidates for microbial electrosynthesis, a process in which microbes use electricity to produce biocommodities from CO_2 (16–18). Despite continued interest in microbes capable of photoferrotrophy and phototrophic EEU, the mechanisms underlying these processes are poorly understood.

The bacterial outer envelope is nonconductive to electrons and is impermeable to insoluble iron minerals/electrodes (19, 20). Therefore, the ability of phototrophs to use the extracellular electron donors likely involves an extracellular electron uptake (EEU) process. Studies in the nonphototroph model bacterium *Shewanella oneidensis* suggest that the mechanism of electron transfer across the outer membrane (OM) employs a porin-cytochrome complex (21). The *Shewanella* complex is comprised of a porin (MtrB) and two decaheme cytochrome *c* proteins (MtrA and MtrC from periplasmic and extracellular sides, respectively) as an electron conduit. Deletion of the extracellular decaheme cytochrome *c* component of the conduit (MtrC and its paralogues, OmcA and MtrF) abrogates *Shewanella*'s ability to reduce Fe(III) or transfer electrons to electrodes (22–24). Recently, it has been shown that the *Shewanella* MtrCAB conduit may also be employed for electron uptake (electron transfer in the opposite direction from its native function) from a cathode to an intracellular reduction reaction (18, 25). In contrast to oxidation of insoluble iron/electrode, soluble iron oxidation could occur either extracellularly or in the periplasm of Gram-negative phototrophs (26–28). Evidence to date suggests that the oxidation of soluble iron in *Rhodopseudomonas palustris* TIE-1 (6) and *Rhodobacter* sp. strain SW2 (29) involves periplasmic iron oxidoreductases (PioA and FoxE, respectively). However, the oxidation of soluble iron could be extracellular because the product of this process is insoluble iron, which can be toxic if produced in the periplasm (10, 13, 30, 31). Genetic studies in *R. palustris* TIE-1, the only genetically tractable phototroph (32) that can perform both photoferrotrophy and phototrophic EEU (6, 7, 15), identified the *pioABC* operon as required for both of these processes (6, 15). The operon encodes PioA, a decaheme cytochrome *c* (cyt *c*), PioB, an outer membrane (OM) porin, and PioC, a high-potential iron-sulfur protein (HiPIP). A deletion mutant lacking *pioABC* cannot perform photoferrotrophy (6) and has a partial defect in phototrophic EEU (15). Beyond these genetic studies, only the iron-sulfur protein PioC has been biochemically characterized as a periplasmic electron transfer protein and proposed to shuttle electrons from PioA to the photosynthetic reaction center (33, 34). However, where Pio proteins oxidize Fe(II) during photoferrotrophy and how they transfer electrons across the outer membrane from poised electrodes during phototrophic EEU are unknown.

Here, we show that PioA undergoes novel postsecretory proteolysis of its N terminus to produce a decaheme-attached PioA (holo-$PioA_C$, where $PioA_C$ represents the C terminus of PioA). The holo-$PioA_C$ is an iron oxidoreductase that forms a membrane-associated protein complex with PioB. The holo-$PioA_C$B complex acts as an electron conduit in TIE-1 to accept electrons from the extracellular oxidation of both Fe(II) and from the poised electrodes (that mimic insoluble iron minerals). Importantly, this process employs a single decaheme cyt *c* (holo-$PioA_C$) and a porin (PioB), with no apparent extracellular electron transfer protein. Therefore, the PioAB complex is distinct from other porin-cytochrome *c* systems found in nonphototrophic bacteria. The postsecretory proteolysis of the N-terminal extension of PioA-like homologs to produce a functional holo-$PioA_C$ and the formation of holo-$PioA_C$B electron conduit are conserved in phototrophs such as *Rhodomicrobium vannielii* and *Rhodomicrobium udaipurense*. Together, these results suggest that the PioAB system can serve as a molecular signature for photoferrotrophy and phototrophic EEU.

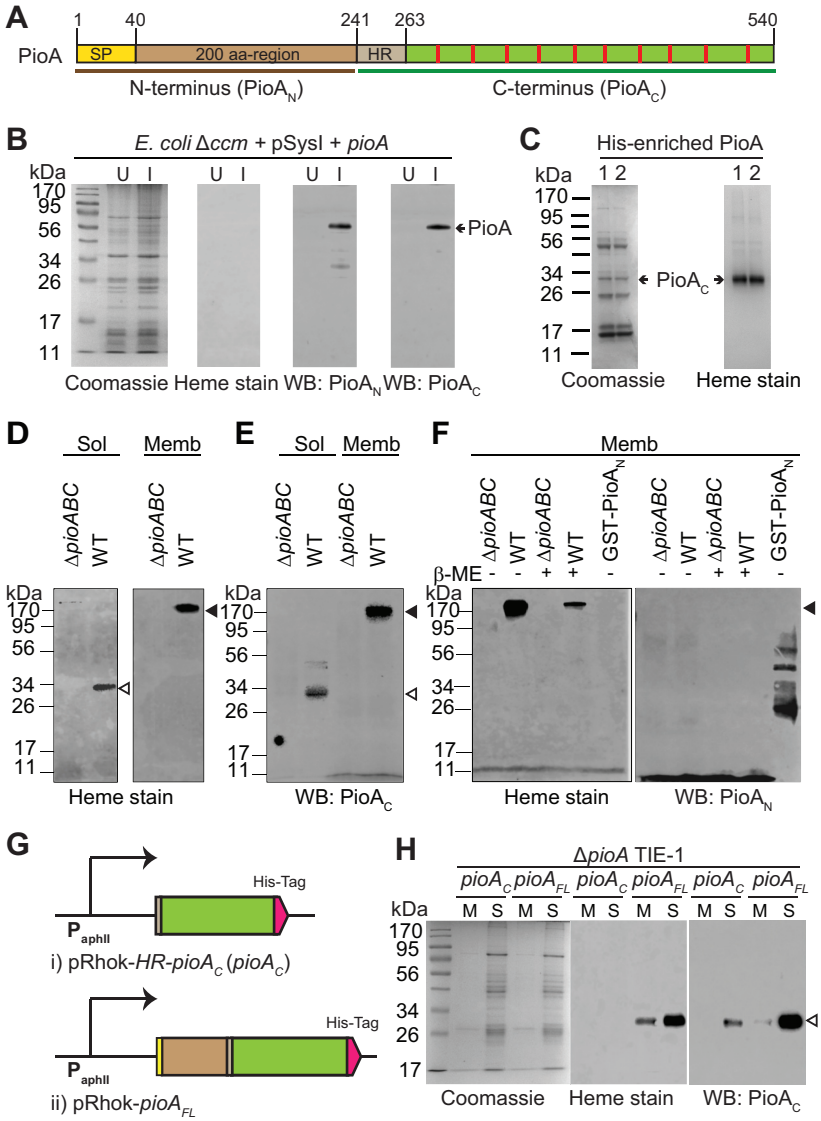

FIG 1 A 34-kDa holo-PioA$_C$ is produced both in TIE-1 and *E. coli*. (A) Schematic diagram of the annotated PioA sequence representing N and C termini of PioA. SP, predicted Sec signal peptide; HR, hydrophobic region; red strip, a heme binding site. (B and C) PioA expression and analysis in *E. coli*. Results of Coomassie and heme staining and Western blotting (WB) with PioA-specific antibodies (anti-PioA$_N$ and anti-PioA$_C$) of total cell lysate of uninduced (U) and induced (I) cells are shown in panel B. Arrow, ~54-kDa PioA. Results of Coomassie and heme staining of His-enriched PioA are shown in panel C. Arrow, heme-stainable PioA (~34 kDa, PioA$_C$). Lanes 1 and 2 represent two replicates. (D to H) PioA analysis in TIE-1. Heme staining (D) and immunoblotting with anti-PioA$_C$ antibodies (E) of the soluble (Sol) and membrane (Memb) fractions from wild type (WT) and Δ*pioABC* mutant are shown. Mass spectrometry analysis of the >170-kDa (membrane fraction) PioA bands identified it as PioAB complex (Fig. S4A). Heme staining and immunoblotting with anti-PioA$_N$ antibodies for the membrane fractions of WT and Δ*pioABC* mutant are shown in panel F. Treatment with β-mercaptoethanol (β-ME) to help unfold the PioAB complex is indicated. An affinity-purified glutathione *S*-transferase (GST)-PioA$_N$ fusion protein was used as a positive control. Schematics of the constructs expressing either only the C terminus of PioA (HR-PioA$_C$) (i) or a full-length PioA (PioA$_{FL}$) with a C-terminal His tag under P$_{aphII}$, a constitutive promoter (ii) are shown in panel G. Coomassie and heme staining and immunoblotting with anti-PioA$_C$ antibodies on His-enriched PioA from membrane (M) and soluble (S) fractions of a Δ*pioA* TIE-1 mutant expressing either HR-PioA$_C$ or PioA$_{FL}$ are shown in panel H. A Coomassie gel was run to ensure nearly equal protein loading. Open and filled triangles indicate holo-PioA$_C$ (~34 kDa) and holo-PioA$_C$B complex (>170 kDa), respectively.

RESULTS AND DISCUSSION

Production and purification of recombinant PioA from *Escherichia coli*. The *pioA* gene (Rpal_0817) encodes a 540-amino-acid (aa) decaheme cyt *c* with a canonical signal peptide (SP; aa 1 to 40), a 200-residue N terminus, and the C terminus (Fig. 1A).

The C terminus contains a hydrophobic region (HR; aa 241 to 263) followed by 10 sites for *c*-type heme (CXXCH) attachment (Fig. 1A). PioA has a large (~200 aa) N terminal region not present in previously characterized decaheme cyt *c* homologs such as MtrA and MtoA (see Fig. S1 in the supplemental material). This N-terminal extension is conserved in PioA homologs annotated in the genomes of different phototrophic bacteria and does not harbor any clear protein domains (Fig. S2). Previous translational fusion studies suggest that a full-length PioA with its N terminus is produced in TIE-1 (35). Here, we wanted to investigate the role of the N terminal extension in these decaheme homologs by studying PioA. Although PioA expression in TIE-1 is upregulated only under photoferrotrophy, its slow growth (doubling time of 80 ± 10 h) and low biomass yields under this condition make it difficult to purify sufficient protein for biochemical analysis.

We heterologously expressed PioA with a C-terminal His tag in the *E. coli* (Δ*ccm*) RK103 strain carrying the *ccmABCDEFGH* genes under an inducible promoter to ensure heme attachment (36). For correct localization of the protein in *E. coli*'s periplasm, we replaced the PioA signal peptide with a validated signal peptide of the cytochrome c_4 gene (36). We confirmed production of the predicted full-length apo-PioA (~54 kDa) in total *E. coli* lysate by immunoblotting with antibodies specific to the N-terminal 200-aa region (anti-$PioA_N$) and the C terminus (anti-$PioA_C$) of PioA (Fig. 1B). However, an ~34-kDa heme-containing polypeptide was observed upon enrichment using hexahistidine affinity purification (Fig. 1C). Heme stains were used to detect covalently bound (*c*-type) heme in the protein (37). The polypeptide was immunodetected with anti-$PioA_C$ but not with anti-$PioA_N$ antibodies (Fig. S3A). These results suggest that the 34-kDa protein is PioA after removal of the N-terminal 200-aa region. Here, the recombinant holo-PioA is termed holo-$PioA_C^r$.

TIE-1 produces a 34-kDa holo-$PioA_C$ that exists as a free periplasmic protein and in a complex with PioB. To investigate the biological relevance of PioA N-terminal processing in the native photosynthetic host, we isolated soluble and membrane fractions of photoautotrophically grown wild-type (WT) and Δ*pioABC* mutant strains of TIE-1. We observed two heme-containing polypeptides: an ~34-kDa band in the soluble fraction and a larger (>170-kDa) band in the membrane fraction of WT TIE-1 (Fig. 1D). Both bands reacted with anti-$PioA_C$ antibodies (Fig. 1E) but not with anti-$PioA_N$ antibodies (Fig. 1F). Mass spectrometry analysis of these bands identified only the C-terminal peptides of PioA, consistent with processing of the N-terminal region in these heme-attached forms of PioA. These results suggest that TIE-1 produces only the 34-kDa heme-attached C terminus of PioA (here termed holo-$PioA_C$). Mass spectrometry analysis of the >170-kDa protein band identified it as $PioA_CB$ complex (Fig. S4A). This band also demonstrates heat modifiability (Fig. S4B), a feature reported for bacterial porins (38–42). Indeed, the holo-$PioA_CB$ migrates as an ~120-kDa band without heat treatment and shifts to >170 kDa when the sample is heated to 90°C for 3 min (Fig. S4B). The 120-kDa holo-$PioA_CB$ band (unheated) likely represents the observed size of holo-$PioA_C$ (~34 kDa) plus the expected size of PioB (~87 kDa), further indicating that the complex is composed of holo-$PioA_C$ (that lacks the N-terminal region) and PioB. Overall, these results suggest that TIE-1 produces a 34-kDa holo-$PioA_C$ that exists in two forms, a free soluble periplasmic protein and a membrane-associated protein in complex with PioB (holo-$PioA_CB$).

Holo-$PioA_C$ produced natively in TIE-1 is the same size as holo-$PioA_C^r$ produced heterologously in *E. coli* (as determined by SDS-PAGE). A similarly sized heme-stainable PioA (~40 kDa) was previously observed from the soluble fraction of TIE-1 by Jiao and Newman (6). The size observed for holo-$PioA_C$ is comparable to the size of the previously characterized decaheme homologs MtrA and MtoA (21, 31). Our biochemical results suggest that holo-$PioA_C$ is the functional component of a $PioA_CB$ complex in TIE-1. However, holo-$PioA_C$ lacks the N-terminal 200-aa region of the predicted PioA protein. The question remains as to how TIE-1 produces holo-$PioA_C$. There are two possibilities: (i) full-length PioA is produced and processed to produce holo-$PioA_C$, or (ii) an internal methionine closer to the first heme attachment site is the functional start

codon. Interestingly, the internal hydrophobic region (HR) of the C terminus of PioA starts with a methionine residue (Met241), and Met241 is the only internal methionine from which a putative Sec signal peptide is predicted based on PredTat (43). It is therefore possible that Met241 is used as a start codon for PioA, with the Sec signal in the HR serving as a periplasmic signal peptide and with the resulting protein being ~34 kDa. There is, however, no observable canonical ribosome binding site (RBS) upstream of Met241. To directly test this possibility, we expressed the *pioA* gene encoding only the C terminus of PioA from the HR (241 to 540 aa; HR-PioA$_C$) with a C-terminal 6×His tag in the Δ*pioA* mutant using a pRhokS-2 plasmid under a constitutive promoter, P*aphII*, along with a strong RBS (Fig. 1G) (44). We observed (by PioA$_C$ Western blotting [WB]) the expected size of HR-PioA$_C$ upon enrichment using hexahistidine affinity purification, suggesting that this version of the protein can be produced artificially in TIE-1 (Fig. 1H, WB:PioA$_C$). However, HR-PioA$_C$ was not heme attached as determined by heme staining (Fig. 1H, PioA$_C$). Because *c*-heme maturation will depend on the periplasmic transport of HR-PioA$_C$, the above result suggests that the Sec signal within the HR is not a functional periplasmic signal and that Met241 does not serve as an alternative start codon for PioA. These results demonstrate the importance of the N terminus (signal peptide and 200-aa region) in the synthesis of holo-PioA$_C$ in TIE-1.

N-terminal processing of PioA is required for photoferrotrophy. To gain insights into the biological role of N-terminal processing, we engineered a series of N-terminal-PioA chromosomal deletion mutants in TIE-1 (Fig. 2A). We tested the ability of these mutants to perform Fe(II) oxidation. The Δ240 mutant lacks the complete N terminal region that includes both the predicted signal peptide and the 200-aa region, the Δ43 mutant lacks only the signal peptide, and the Δ200 mutant lacks only the 200-aa region but contains the intact signal peptide. Photoautotrophically grown TIE-1 cells with hydrogen were used for cell suspension assays. We observed that the Δ200 mutant oxidized Fe(II) both in the cell suspension assays and during photoferrotrophy (Fig. 2B and C, green line, and Fig. S5). In contrast, the Δ240 and Δ43 mutants, which lack the signal peptide that is essential for periplasmic export, were unable to oxidize Fe(II) or perform photoferrotrophy (Fig. 2B and C, red and purple lines, respectively). Furthermore, only the Δ200 construct rescued the phenotype of a Δ*pioA* mutant when expressed in *trans* from a plasmid (Fig. 2D). The ability of the Δ200 mutant to oxidize Fe(II) suggests that holo-PioA$_C$ is a functional iron oxidase in TIE-1. It also demonstrates that the N-terminal 200-aa region of PioA is not directly involved in the ability of PioA to oxidize Fe(II).

Although the Δ200 mutant was able to grow via photoferrotrophy, it had an extended lag phase compared to that of the WT (Fig. 2C). We examined whether this lag is due to the difference in PioA concentrations between these two strains. To approximate photoferrotrophy and obtain sufficient cells for total protein extraction, strains grown photoautotrophically with hydrogen (optical density at 660 nm [OD$_{660,}$] of 1.0) were exposed to 3 mM Fe(II) and harvested after 22 h when all Fe(II) was oxidized (Fig. 2E). We observed a smaller amount of both free holo-PioA$_C$ and holo-PioA$_C$B complex in the Δ200 mutant than in the WT (Fig. 2F and G). We also assessed the relative transcript levels of *pioA* under these conditions and observed a slight increase in *pioA* transcripts in the Δ200 mutant compared to the level in the WT (Fig. 2H). This result rules out the possibility that the lower level of free holo-PioA$_C$ and holo-PioA$_C$B complex in the Δ200 mutant could be due to lower protein expression in the mutant. Therefore, we propose that the N-terminal 200-aa region of PioA plays a role in maintaining the concentration of holo-PioA$_C$ in TIE-1 at wild-type levels. Edman degradation analyses of holo-PioA$_C$ purified from TIE-1 identified Ala243 as the N-terminal residue of the processed protein (Fig. 3). Cleavage at this site would produce a protein with a predicted molecular weight of 34 kDa, as calculated for the holo-PioA$_C$.

N-terminally processed PioA is an iron oxidase. The fact that holo-PioA$_C$ is required for Fe(II) oxidation in TIE-1 suggests that it is an iron oxidoreductase. Thus, we affinity purified holo-PioA$_C^r$ and assayed its iron oxidation capacity by UV-visible light

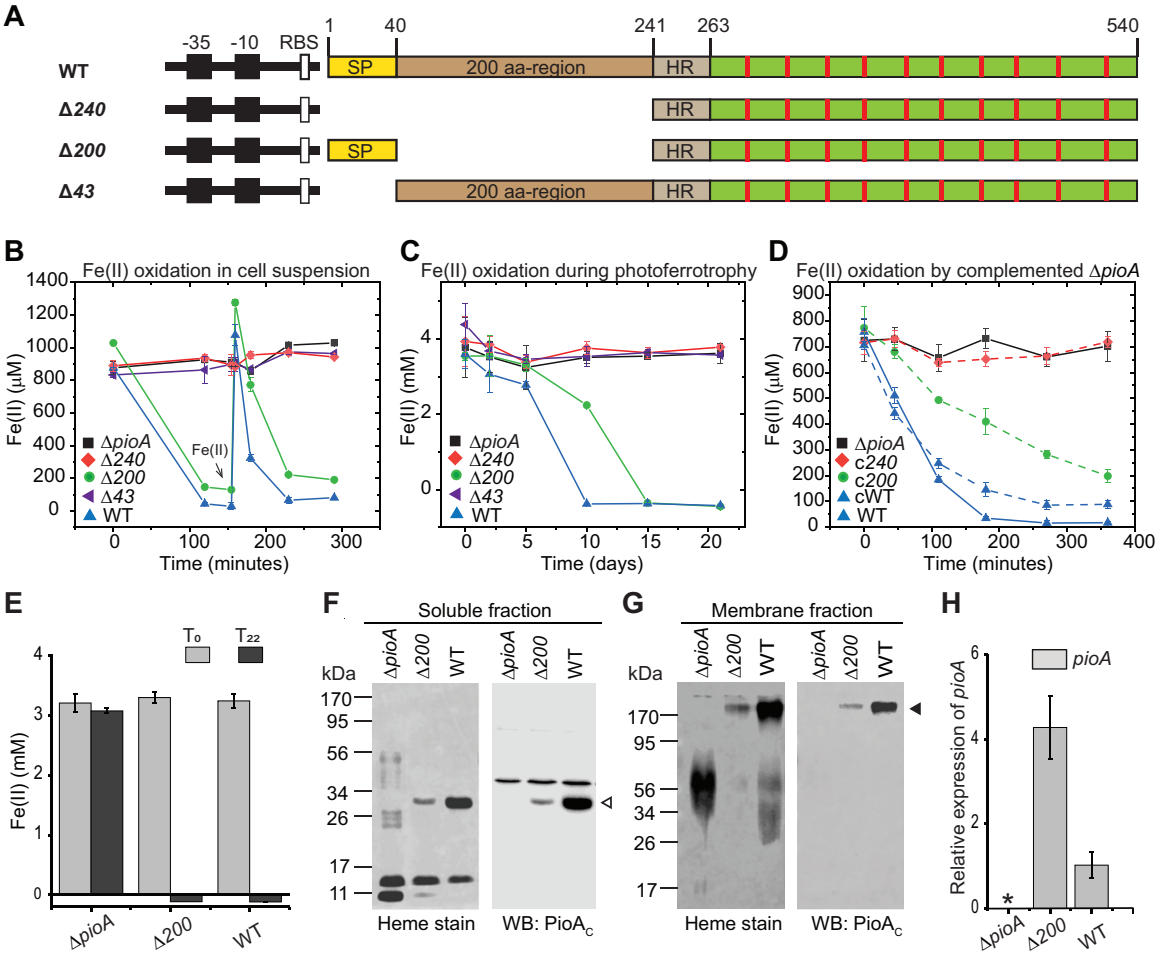

FIG 2 Production of the holo-PioA$_C$ (34 kDa) is required for photoferrotrophy in TIE-1. (A) Schematic representation of the *pioA* gene in the wild-type (WT) TIE-1 and Δ240, Δ200, and Δ43 TIE-1 mutant genomes. The mutants lack regions encoding the N terminus (Δ240), the 200-aa region (Δ200), and the putative signal peptide (Δ43) of PioA protein. (B) Fe(II) oxidation by WT and TIE-1 mutants in cell suspension assays. Data shown are representative of three independent experiments. Error bars are means ± standard deviations of three technical replicates. (C) Fe(II) oxidation by WT and TIE-1 mutants during photoferrotrophic growth. Data are means ± standard deviations of three biological replicates. Cell growth during photoferrotrophy was determined by OD_{660} measurements at indicated time points and protein quantification at the initial (T_0) and final (T_f) time points (Fig. S5). (D) Complementation of the Fe(II)-oxidizing ability of Δ*pioA* mutant by expressing *pioA*-containing plasmids that mimic the Δ240, Δ200, and WT genotypes. Data shown are representative of three independent experiments. Error bars are means ± standard deviations of three technical replicates. (E) Fe(II) oxidation by the Δ*pioA* and Δ200 mutants and WT TIE-1. Fe(II) concentration at the initial time (T_0) and after 22 h (T_{22}) of Fe(II) exposure are shown. Error bars are means ± standard deviations of three technical replicates. (F and G) Heme staining and Western blotting (WB) with anti-PioA$_C$ antibodies for the soluble (F) and membrane (G) fractions of cells harvested after 22 h. Upregulation of other cyt *c* proteins was observed for the *pio* mutants compared to expression in the WT. Open and filled triangles indicate holo-PioA$_C$ and holo-PioA$_C$B complex, respectively. (H) Relative expression of *pioA* (normalized to that of *recA*) in cells harvested after 22 h. qRT-PCR data are means ± standard errors for three biological replicates assayed in duplicate. The asterisk represents a low value (0.01) for the Δ*pioA* mutant control.

(UV-Vis) spectroscopy under anaerobic conditions. The UV-Vis spectra of holo-PioA$_C^r$ show the spectral signatures of typical *c*-type cytochromes (Fig. 4A and Fig. S3B). Covalently bound heme in holo-PioA$_C^r$ was determined by observing a 550-nm α peak in the pyridine hemochrome assay (Fig. 4A, inset) (45, 46). The dithionite-reduced holo-PioA$_C^r$ (Fig. 4A, purple) was reoxidized after addition of Fe(III) chloride solution, as indicated by a shift of the Soret peak back from 418 to 408 nm and disappearance of the α and β peaks at 551 and 523 nm, respectively (Fig. 4A, teal blue). This spectral characteristic of holo-PioA$_C^r$ is similar to that of the reduced-MtrCAB complex after addition of Fe(III) citrate (21). As reported for the decaheme cyt *c* MtoA (31), the reduction of holo-PioA$_C^r$ with Fe(II) chloride was pH dependent and only detected at a basic pH of 9 to 10 (Fig. 4B). These results demonstrate that holo-PioA$_C^r$ can donate electrons to Fe(III) and accept electrons from Fe(II). Thus, the N-terminal 200-aa region

FIG 3 PioA is processed at Ala243 in the hydrophobic region. (A) Coomassie and heme staining of affinity-purified holo-PioA$_C$ from the Δ*pioA* TIE-1 mutant expressing full-length *pioA* under the *pio* promoter with a C-terminal His tag. The band corresponding to the heme band (34 kDa, boxed) from the Coomassie blot was used for Edman degradation analysis (5-aa N-terminal sequencing). (B) PioA sequence showing N-terminal amino acids determined in Edman analysis of 34-kDa holo-PioA$_C$ (ATREPR, underlined). The arrowhead indicates a cleavage site between Val242 and Ala243. Colors of peptides are consistent with the colors of different regions (Sec signal, 200-aa, HR, and heme-binding C terminus) of PioA represented in the models in Fig. 1A and 2A. The peptides detected by mass spectrometry analysis of the 34-kDa PioA band are highlighted.

of PioA is not required for iron oxidase activity, but its processing is required for proper attachment of the heme groups to PioA, suggesting a regulatory role during PioA maturation.

The holo-PioA$_C$B complex catalyzes the extracellular oxidation of iron *in vivo*. An important unknown aspect of photoferrotrophy is the location of the Fe(II) oxidation activity in the bacterial cell. Our results suggest that Fe(II) oxidation could occur either in the periplasm by soluble holo-PioA$_C$ or extracellularly by the holo-PioA$_C$B complex. Both activities could also occur simultaneously in TIE-1. To dissect the roles of soluble holo-PioA$_C$ and holo-PioA$_C$B complex, we used the TIE-1 Δ*pioB* mutant. Deletions of *pioA*, *pioB*, and *pioC* in TIE-1 have been shown to be nonpolar (6). First, we tested the fate of holo-PioA$_C$ in the absence of the PioB protein. Analysis of holo-PioA$_C$ in the Δ*pioB* mutant showed that the protein is present only in the soluble fraction and not in the membrane fraction (Fig. 5A). This result agrees with the bioinformatic prediction of PioA as a periplasmic soluble protein and reveals the importance of PioB in the

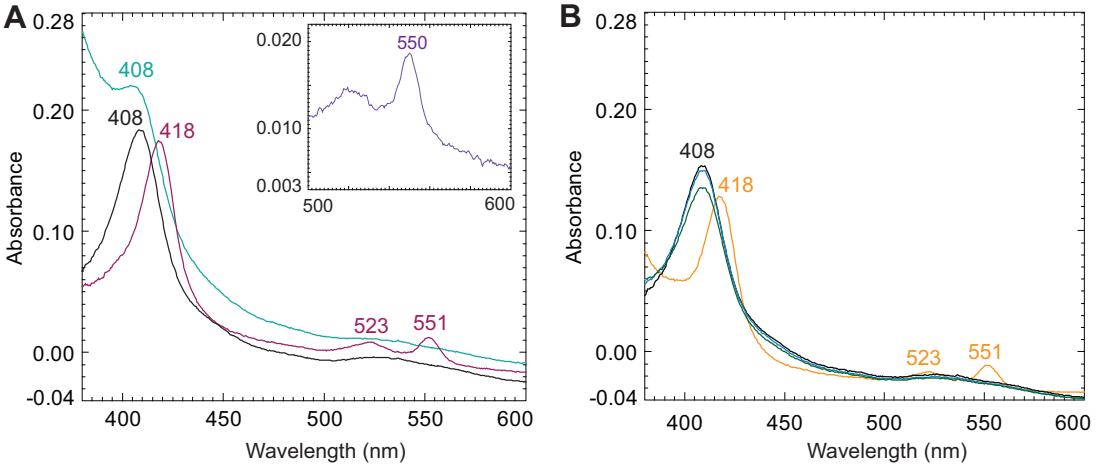

FIG 4 The holo-PioA$_C$ is an iron oxidoreductase. UV-visible light spectral analysis of the affinity-purified PioA$_C^r$ was performed under anaerobic conditions. (A) Purified PioA (black), PioA reduced with sodium dithionite (purple), and reoxidized PioA (teal blue) after addition of Fe(III) chloride solution (100 μM) to reduced-PioA. The inset shows a pyridine hemochrome assay. (B) Purified PioA (black), PioA after addition of Fe(II) chloride solution (blue), PioA after increasing the pH to ~8 (dark green), and PioA after increasing pH to ~9 to 10 (orange).

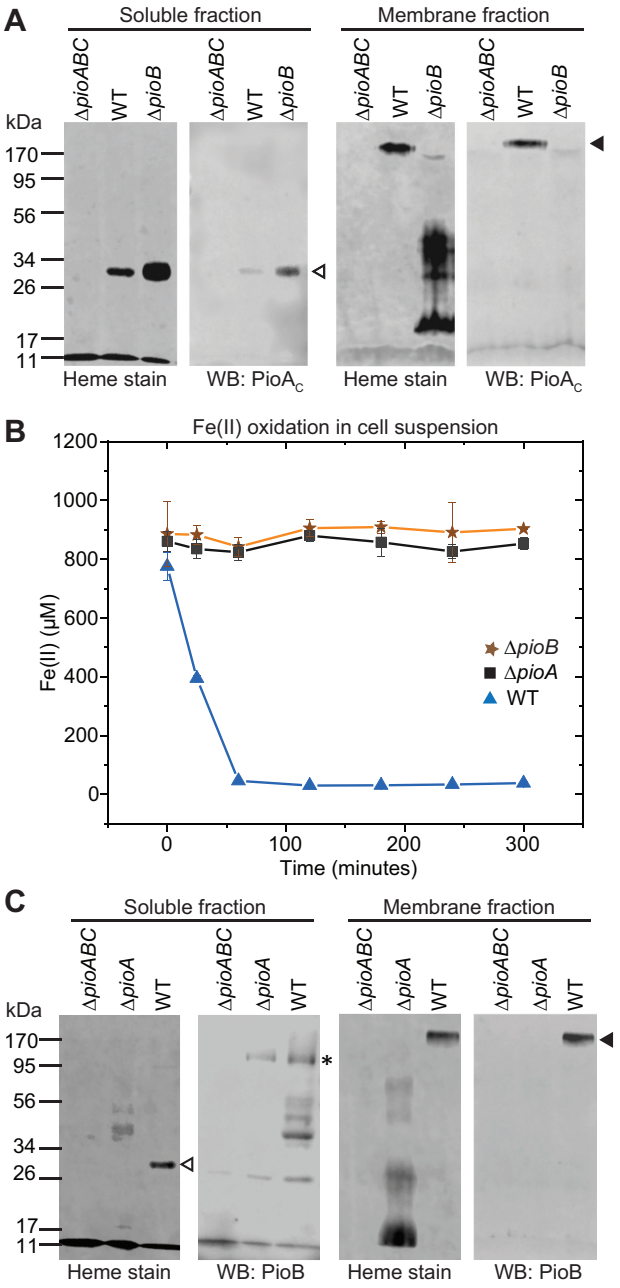

FIG 5 PioA and PioB codependence for outer membrane incorporation. (A) Heme staining and anti-PioA$_C$ Western blotting (WB) of proteins in the soluble and membrane fractions of the Δ*pioABC* mutant, WT, and Δ*pioB* mutant. Open and filled triangles indicate holo-PioA$_C$ and holo-PioA$_C$B complex, respectively. (B) Fe(II) oxidation by the WT and the Δ*pioABC* and Δ*pioB* mutants in cell suspension assays. Data shown are representative of three independent experiments. Error bars are means ± standard deviations of three technical replicates. (C) Heme staining and immunoblotting with anti-PioB antibodies for the soluble and membrane fractions of the Δ*pioABC*, Δ*pioA*, and WT strains. The asterisk indicates free PioB.

localization of PioA to the membrane. Because the Δ*pioB* mutant contains only soluble holo-PioA$_C$, it serves as an ideal construct to investigate the role of periplasmic soluble holo-PioA$_C$ in Fe(II) oxidation. We found that Δ*pioB* cannot oxidize Fe(II) in cell suspension assays (Fig. 5B). Because periplasmic holo-PioA$_C$ is produced in the Δ*pioB* mutant, this result indicates that Fe(II) oxidation is unlikely to be carried out by soluble holo-PioA$_C$ in the periplasm. Another explanation for this result might be that PioB acts as an Fe(II) import porin that makes Fe(II) available to periplasmic PioA for iron

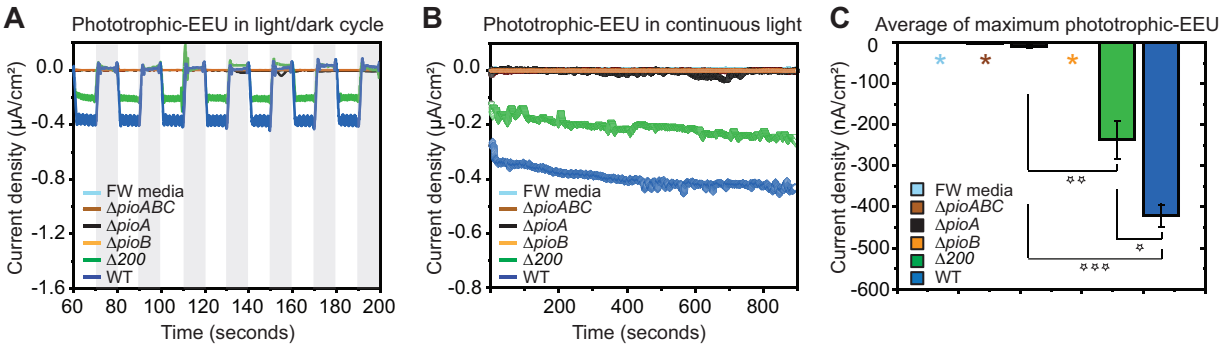

FIG 6 The holo-PioA$_C$B complex is responsible for phototrophic EEU in TIE-1. Electron uptake (represented as current density) by the Δ*pioABC*, Δ*pioA*, Δ*pioB*, Δ200, and WT TIE-1 strains in the microfluidic bioelectrochemical cell (μ-BEC) under a light-dark cycle (shaded region) (A) and under continuous light (B) are shown. Data shown are representative of three experiments. (C) Average maximum electron uptake under continuous light at a time point of 600 s is represented as a bar diagram. Asterisks represent low current density values for a no-cell control (FW medium, 0.16 nA/cm^2), Δ*pioABC* mutant (−1.31 nA/cm^2), and the Δ*pioB* mutant (−0.45 nA/cm^2). Error bars are means ± standard deviations of three biological replicates. The *P* values were determined by Student's *t* test (1 star, $P < 0.05$; 2 stars, $P < 0.01$; 3 stars, $P < 0.001$).

oxidation and/or as an Fe(III) export porin to remove Fe(III) from the cell. This would prevent accumulation of iron oxides in the periplasm, likely a lethal event for the cell (6). However, based on precedence from the MtrAB system in *Shewanella* (21, 47), PioB might exist only as a PioAB complex in the outer membrane. Moreover, in the MtrAB system in *Shewanella*, MtrB requires MtrA to enter the outer membrane (OM), and, therefore, the two proteins are inserted into the OM as a MtrAB complex (21, 47). To this end, we investigated the fate of PioB in the absence of PioA by using a Δ*pioA* mutant. Similar to observations of MtrAB, using immunoblotting with an antibody specific to PioB, we observed the presence of PioB in the soluble fraction but not in the membrane fraction of the Δ*pioA* mutant (Fig. 5C). This result suggests that the holo-PioA$_C$ and PioB localize together as a complex in the OM, and, therefore, PioB is likely not present as a discrete porin in TIE-1. This result is further supported by the fact that we could detect only the holo-PioA$_C$B complex and not free PioB in the membrane fraction of WT TIE-1 (Fig. 5C). Together, these results suggest that it is unlikely that soluble holo-PioA$_C$ performs periplasmic Fe(II) oxidation and supports the hypothesis that the holo-PioA$_C$B complex catalyzes Fe(II) oxidation extracellularly.

The holo-PioA$_C$B complex is required for phototrophic EEU in TIE-1. In addition to Fe(II), TIE-1 can oxidize insoluble iron minerals, such as hematite (7), and electrodes poised at the potential of insoluble iron minerals (15). Because these insoluble electron donors cannot cross the bacterial envelope, they are most likely oxidized by TIE-1 extracellularly via the holo-PioA$_C$B complex. Poised electrodes in bulk reactors have been used as proxies of natural interactions between microbes and minerals such as iron oxides (15, 48, 49). However, in such bulk reactors different factors, such as extracellular enzymes (50), presence of planktonic cells, mediators, and abiotic reactions, could affect the electrochemical signals (15, 51). Therefore, we examined the involvement of the holo-PioA$_C$B complex in EEU using a microfluidic bioelectrochemical cell (μ-BEC) developed in our laboratory (14). In the μ-BEC, an electrode poised at +100 mV versus a standard hydrogen electrode (SHE) was used to mimic the redox potential of insoluble iron minerals (15). We monitored and compared the light-dependent electron uptake ability of WT TIE-1 and mutants. Intermediate electron uptake by the Δ200 mutant was observed compared to that of the WT TIE-1 (Fig. 6A to C, green and blue, respectively; Table S1). This corroborates the observation that the Δ200 mutant contains a smaller amount of holo-PioA$_C$B complex (Fig. 2G). We did not detect electron uptake by either the Δ*pioABC or* Δ*pioA* mutant. Similar to findings with respect to Fe(II) oxidation, Δ*pioB* mutant could not perform phototrophic EEU (Fig. 6A to C, light brown). This result shows that the holo-PioA$_C$B complex, but not free periplasmic holo-PioA$_C$, is responsible for phototrophic EEU in TIE-1. Phototrophic EEU has been studied in bulk bioelectrochemical systems (BESs) (15) and in μ-BECs (14). In

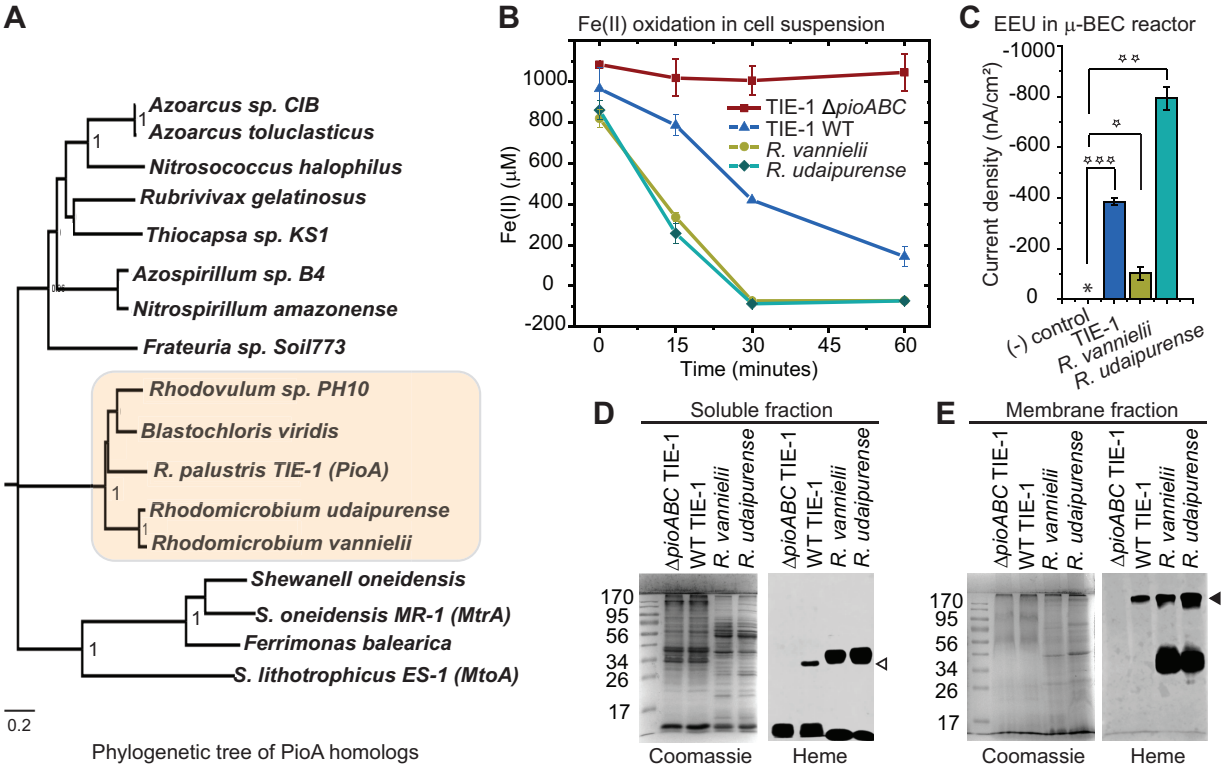

FIG 7 Phototrophic bacteria, *Rhodomicrobium vannielii* DSM 162 and *R. udaipurense* JA643, produce a PioAB complex and perform Fe(II) oxidation and phototrophic EEU. (A) Neighbor-joining phylogenetic tree of decaheme cyt *c* homologs of MtrA-like and PioA-like proteins. The highlighted clade contains a group of phototrophs that contains only PioA-like decaheme homologs. The clade clusters in the same way even when the N-terminal domain is excluded from the alignment. (B) Fe(II) oxidation by *R. vannielii* DSM 162 and *R. udaipurense* JA643 in cell suspension assays. Data shown are representative of three independent experiments. Error bars are means ± standard deviations of three technical replicates. Wild-type TIE-1 and the Δ*pioABC* mutant were used as the positive and negative controls, respectively. (C) Maximum phototrophic EEU (represented as current density) by *R. vannielii* DSM 162 and *R. udaipurense* JA643 in a microfluidic bioelectrochemical cell (μ-BEC) under continuous light. Asterisk represents a low average current density (0.0046 nA/cm^2) for a no-cell negative (−) control. Error bars are means ± standard deviations of three biological replicates. The *P* values were determined by Student's *t* test (1 star, $P < 0.05$; 2 stars, $P < 0.01$; 3 stars, $P < 0.001$). (D and E) Coomassie and heme staining for the soluble and membrane fractions, as indicated, of H_2CO_2 grown TIE-1 Δ*pioABC*, WT TIE-1, *R. vannielii* DSM 162, and *R. udaipurense* JA643. Open and filled triangles indicate a smaller heme-stainable band (like holo-PioA$_C$) in the soluble fraction and a higher-molecular-mass band of >170 kDa (like holo-PioA$_C$B complex) in the membrane fraction, respectively. Mass spectrometry analysis of >170-kDa heme-stainable bands from *R. vannielii* DSM 162 and *R. udaipurense* JA643 confirm the presence of PioA and PioB homologs from the respective bacteria (see Fig. S6 in the supplemental material).

BESs, both planktonic cells (70% electron uptake) and biofilm-attached cells (30% electron uptake) contribute to phototrophic EEU (14, 15). The μ-BEC collects data only from biofilm-attached cells. Therefore, our results from the μ-BEC suggest that in biofilm-attached cells, the PioABC system is essential for phototrophic EEU. This supports previous results from bulk BESs where the Δ*pioABC* mutant lost 30% electron uptake ability (15). Overall, our results indicate that the holo-PioA$_C$B complex serves as an electron conduit in TIE-1 to take up electrons from poised electrodes that mimic insoluble iron minerals.

Postsecretory processing of PioA and holo-PioA$_C$B complex formation is a conserved trait in other phototrophs. Homologs of PioA/MtrA and PioB/MtrB occur as operons in the genomes of many proteobacteria (15, 21). Sequence alignment of decaheme homologs separates them out into two groups, one without the N-terminal extension (MtrA-like) and other with the N-terminal extension (PioA-like) (Fig. S2B). Additionally, phylogenetic analysis clusters bacteria with PioA-like homologs in a distinct clade (Fig. 7A, highlighted clade). Interestingly, this clade includes phototrophic bacteria known to be photoferrotrophs such as TIE-1 (32) and *Rhodomicrobium vannielii* (52). Although the N-terminal extensions vary in length and are not conserved at the level of amino acid sequence, the presence of a larger N terminal region and an internal

hydrophobic region (HR) upstream of the first heme-binding motif are conserved features of PioA-like homologs (Fig. S2B). Our data from TIE-1 has established that the N-terminal region of PioA is important to produce a functional iron oxidoreductase (holo-PioA$_C$) and, hence, the holo-PioA$_C$B complex. To investigate the functional parallels of holo-PioA synthesis and PioAB complex formation in phototrophs, we studied *Rhodomicrobium vannielii* and *Rhodomicrobium udaipurense*. Both of these organisms have PioABC homologs. *R. vannielii* can perform phototrophic Fe(II) oxidation (52) while the ability of *R. udaipurense* to oxidize Fe(II) is unknown. The ability of *R. vannielii* and *R. udaipurense* to perform phototrophic EEU is also unknown.

First, we studied the ability of *R. vannielii* DSM 162 (53) and *R. udaipurense* JA643 (54) to oxidize Fe(II) and perform phototrophic EEU. Both *R. vannielii* DSM 162 and *R. udaipurense* JA643 oxidized Fe(II) in cell suspension assays (Fig. 7B, chartreuse green and teal blue, respectively). We also observed that these phototrophs, similar to TIE-1, can perform phototrophic EEU from an electrode poised at +100 mV versus SHE in a μ-BEC reactor (Fig. 7C and Table S1) (14). Photoautotrophically grown *R. vannielii* DSM 162 and *R. udaipurense* JA643 with hydrogen were used for cell suspension assays, and their ability to oxidize Fe(II) suggests that the iron oxidase (PioA homologs) is produced under this growth condition. To investigate whether these phototrophs, like TIE-1, also synthesize holo-PioA$_C$ and holo-PioA$_C$B complex, cell fractions of photoautotrophically grown *R. vannielii* DSM 162 and *R. udaipurense* JA643 were analyzed. Heme staining of the soluble and membrane fractions from these bacteria showed band patterns similar to those of TIE-1. We observed two heme-stainable bands, an ~34-kDa band in the soluble fraction and a >170-kDa band in the membrane fraction (Fig. 7D and E), for both phototrophs. The >170-kDa bands from *R. vannielii* DSM 162 and *R. udaipurense* JA643 were confirmed to contain PioA and PioB homologs by mass spectrometry analysis (Fig. S6). Interestingly, these bacteria also contain a smaller holo-PioA (~34 kDa) in the soluble fraction than expected (~48 kDa) from their annotated sequences (Fig. 7D). Furthermore, only the C-terminal peptides of the PioA homologs were detected by the mass spectrometry of these heme-stainable PioAB complexes (>170 kDa). Together, these results suggest that the PioA-like homologs in *R. vannielii* DSM 162 and *R. udaipurense* JA643, similar to the PioA of TIE-1, undergo postsecretory proteolysis of the N-terminal region to produce a smaller holo-PioA$_C$.

A holo-PioA$_C$B complex as the cornerstone for photoferrotrophy and phototrophic EEU. Our biochemical and genetic studies show that the holo-PioA$_C$B complex is responsible for extracellular oxidation and electron uptake from both soluble Fe(II) and poised electrodes (that mimic insoluble iron minerals). The molecular mechanism of electron transfer by a porin and a single decaheme protein, as in the holo-PioA$_C$B complex in TIE-1, is not well understood. To investigate whether the dimensions of predicted models of holo-PioA$_C$ and PioB could support the formation of a holo-PioA$_C$B complex to allow EEU to occur across the OM, we performed *in silico* analysis of PioA$_C$ and PioB using RaptorX, a web-based server for protein structure prediction (55). The predicted structure of holo-PioA$_C$ has the dimensions of ~100 by 40 by 30 Å (Fig. S7A and B), and the predicted structure of PioB has an estimated pore diameter of ~30 to 40 Å (Fig. S7C and D). Although cryo-electron microscopy (cryo-EM) or crystal structures will be necessary to validate the topology and structure of PioA$_C$B, these *in silico* structure predictions suggest a holo-PioA$_C$B model (Fig. 8A and Fig. S7E) where holo-PioA$_C$ inserts through the entire length of PioB and supports EEU across the OM (~40 to 50 Å in width) of TIE-1.

Conclusions. The results support a model (Fig. 8B) for the synthesis and function of key proteins involved in photoferrotrophy and phototrophic EEU whereby the cytoplasmic PioA precursor (540 aa) is exported to the periplasm via the Sec pathway with the concomitant removal of its signal peptide (1 to 40 aa) (56). The periplasmic apo-PioA (500 aa) is then proteolytically processed at the Ala243 site by a periplasmic/membrane protease to facilitate heme attachment and produce holo-PioA$_C$ (297 aa, 34 kDa). Holo-PioA$_C$ exists in two forms, in a free periplasmic form and in a complex with

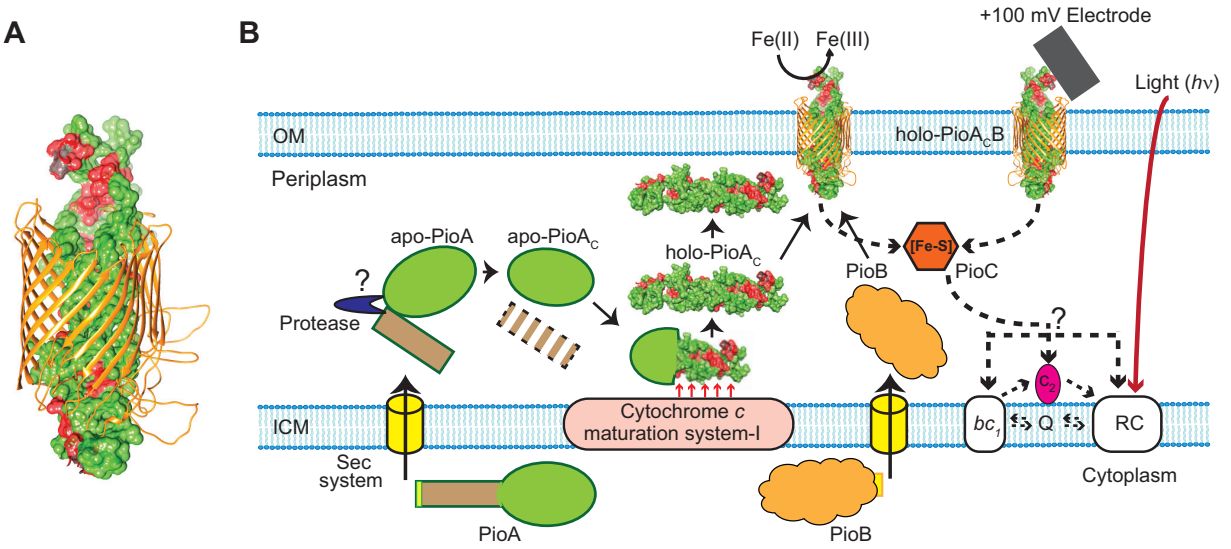

FIG 8 Proposed model for PioA$_C$B complex synthesis and function. (A) *In silico*-predicted model for holo-PioA$_C$B complex. (B) A model for assembly of the active holo-PioA$_C$B complex. The model describes the postsecretory steps in the synthesis of holo-PioA$_C$ and demonstrates an electron uptake mechanism via PioA$_C$B complex that enables *R. palustris* TIE-1 to utilize both Fe(II) and poised electrodes that mimic insoluble iron minerals as electron donors for photosynthesis. PioC, a periplasmic high-potential iron-sulfur (Fe-S) protein, shuttles electrons from the inner face of the holo-PioA$_C$B complex to photosynthetic reaction center. *In silico*-predicted models in panel A and in Fig. S7 in the supplemental material were used to demonstrate folded forms of holo-PioA$_C$, PioB, and the holo-PioA$_C$B complex in this model. Solid arrows, steps in protein transport, processing, and complex formation; dashed arrows, the path of electron transfer; OM, outer membrane; ICM, inner cytoplasmic membrane; Q, ubiquinone pool; bc_1, bc_1 complex; RC, photosynthetic reaction center.

PioB. The free periplasmic form of holo-PioA$_C$ is required for the stability and incorporation of PioB in the OM. Based on the dependency of MtrB on MtrA for its OM localization (21, 47) and the discovery of MtrB with an opposite orientation in the OM (57), it was proposed that the folding and insertion of MtrB to the OM follow a different pathway than a typical β-barrel OM porin in *Shewanella* (57). Here, we propose that the orientation of PioB (Fig. 8 and Fig. S7) and its folding and insertion to the OM in TIE-1 are similar to those of MtrB. The holo-PioA$_C$B complex catalyzes electron uptake from both extracellular electron donors such as Fe(II) and poised electrodes (that mimic insoluble iron minerals). Subsequently, electrons from the holo-PioA$_C$B complex are transferred to the photosynthetic reaction center in the inner cytoplasmic membrane, most likely via PioC (periplasmic soluble iron-sulfur protein), as previously proposed (33, 34).

Although the 500-residue apo-PioA (54 kDa) is most likely secreted into the periplasm, we did not detect this apo-PioA in TIE-1. This lack of detection could be due to the rapid proteolysis of apo-PioA in TIE-1. In *E. coli*, we observed both the 54-kDa apo-PioA and the 34-kDa holo-PioA$_C^r$ (Fig. 1B and C), detecting heme attachment only in the 34-kDa C-terminal PioA. These results suggest that the proteolysis of apo-PioA occurs before heme maturation in both TIE-1 (and other photoferrotrophs) and *E. coli*. We could not detect a PioAB complex containing full-length apo-PioA; so heme maturation of PioA is likely important for formation of the PioAB complex. Our data demonstrate that the deletion of the N-terminal 200-aa region of apo-PioA does not abrogate production of holo-PioA$_C$ in TIE-1. However, it causes a decrease in the cellular concentration of holo-PioA$_C$ and holo-PioA$_C$B complex, likely leading to a lag in photoferrotrophy (Fig. 2C) and an overall reduction in phototrophic EEU (Fig. 6A to C). The 200-aa region of the N terminus of PioA may play a role in maintaining the concentration of holo-PioA$_C$ in TIE-1 at wild-type levels. This region could control the C-terminal PioA secretion rate and/or access to the cyt *c* maturation pathway (i.e., CcmF/H synthetase) (58, 59). The exact function of the N-terminal region will require further investigation. Although the Δ*pioB* mutant can produce soluble holo-PioA$_C$, it did not oxidize Fe(II) (Fig. 5A and B) or perform phototrophic EEU (Fig. 6A to C). This indicates that both of these processes in TIE-1 are catalyzed extracellularly by holo-PioA$_C$B complex (33, 60).

The PioAB system potentially catalyzes electron transfer from extracellular solid substrates, and its broad distribution suggests that this phenotype may also be widespread (15, 21). Interestingly, we found that PioA-like (decahemes with extended N termini) homologs are conserved only in phototrophic bacteria (Fig. 7A and Fig. S2). Although MtrA-like decaheme homologs and the MtrCAB electron conduit have been previously characterized, these proteins are found in nonphototrophic organisms such as *Shewanella* that use extracellular minerals as their terminal electron acceptors. Typically, these proteins allow electrons produced inside the cytoplasm to be transferred to the terminal electron acceptor. However, the MtrCAB conduit in *Shewanella* requires its extracellular decaheme component, MtrC, or its paralogues (OmcA and MtrF) to reduce Fe(III) or to transfer electrons to electrodes (23–25). In contrast, PioA-like homologs are found in phototrophic bacteria, and the PioAB conduit (with no apparent extracellular decaheme cyt *c* component) likely allow electrons to be transferred across the outer membrane from a variety of extracellular electron donors [such as soluble Fe(II), insoluble iron, and insoluble iron mineral proxies such as poised electrodes] (14). Subsequently, PioC transfers electrons from the PioAB conduit to the photosynthetic reaction center (33, 34). The transferred electrons are utilized to produce NAD(P)H that is required for carbon fixation via the Calvin-Bassham-Benson cycle in TIE-1 (14).

MATERIALS AND METHODS

Bacterial strains and plasmids. A complete list of strains, plasmids, and primers used in this study are described in Table S2 in the supplemental material. Bacteria were grown using medium and culture conditions as previously described (14, 15), and details are provided in Text S1.

Fractionation and preparation of soluble and membrane fractions of TIE-1. Photoautotrophically grown *R. palustris* TIE-1 strains with hydrogen in fresh water (FW) medium (10) were used for fractionation. Fractionation was done as previously described (6) with some modifications (see Text S1 in the supplemental material for a complete description of the methods used).

Protein expression and purification. Affinity purification of proteins from *E. coli* and *R. palustris* TIE-1 were performed as previously described (61). *E. coli* RK103 and the *R. palustris* TIE-1 Δ*pioA* mutant were used as the expression hosts (see Text S1 in the supplemental material for a complete description of the methods used).

Antibody production and immunoblots. Antibody production and immunoblotting are described in detail in Text S1.

Cell suspension assay. All cell suspensions were performed in an anaerobic chamber (80% N_2, 15% CO_2 and 5% H_2; Coy Laboratory, Grass Lake, USA) at room temperature as previously described (6, 28, 62). TIE-1 and other strains were inoculated from a prephotoautotrophic culture in FW medium with hydrogen (80% H_2, 20% CO_2) and grown to an OD_{660} of ~0.3. The cells were harvested by centrifugation (10,000 × *g* for 5 min), washed three times with HEPES buffer (50 mM HEPES, pH 7.0, 20 mM NaCl), resuspended, and concentrated to an OD_{660} of ~0.9 in HEPES buffer supplemented with 1 mM Fe(II) and 5 mM nitrilotriacetic acid (NTA). One hundred microliters of the cell suspensions was aliquoted in the 96-well plate. To start the assay, the plate was placed under a 60-W incandescent light at a distance of 25 cm. Fe(II) measurement at the initial time point (time zero [T_0]) was taken before the light source was turned on. All of the Fe(II) measurements were performed using a ferrozine assay (63).

RNA-preparations and RT-qPCR. RNA-preparations and reverse transcription-quantitative PCR (RT-qPCR) were done as previously described (14, 15), and details are provided in Text S1.

Microfluidic bioelectrochemical cell and conditions. The microfluidic bioelectrochemical cells (μ-BECs) were assembled and used as previously described (14) (see Text S1 in the supplemental material for a complete description of the methods used).

SUPPLEMENTAL MATERIAL

Supplemental material for this article may be found at https://doi.org/10.1128/mBio.02668-19.

TEXT S1, DOCX file, 0.02 MB.
FIG S1, PDF file, 0.8 MB.
FIG S2, PDF file, 1.4 MB.
FIG S3, PDF file, 0.9 MB.
FIG S4, PDF file, 1.1 MB.
FIG S5, PDF file, 0.8 MB.
FIG S6, PDF file, 0.9 MB.
FIG S7, PDF file, 2.7 MB.

TABLE S1, DOCX file, 0.01 MB.
TABLE S2, DOCX file, 0.02 MB.

ACKNOWLEDGMENTS

We thank the following members of the Washington University community: Joseph Jez, Petra Levin, Joshua Blodgett, Rajesh Singh, Michael Guzman, Tahina Ranaivoarisoa, and Wei Bai for their helpful comments during this work; Josh Kim for technical assistance; and Marta Wegorzewska for her careful reading of the manuscript. We thank Bradley Evans and Shin-Cheng Tzeng from the Proteomics and Mass Spectrometry Facility, Donald Danforth Plant Science Center.

This work was supported by the following grants to A.B.: The David and Lucile Packard Foundation Fellowship (201563111), a U.S. Department of Energy grant (number DESC0014613), and a U.S. Department of Defense, Army Research Office grant (number W911NF-18-1-0037). A.B. and J.M.M. were also funded by a Collaboration Initiation Grant, an Office of the Vice Chancellor of Research Grant, and an International Center for Energy, Environment and Sustainability Grant from Washington University in St. Louis. R.G.K. is supported by NIH grant GM47909.

REFERENCES

1. Widdel F, Schnell S, Heising S, Ehrenreich A, Assmus B, Schink B. 1993. Ferrous iron oxidation by anoxygenic phototrophic bacteria. Nature 362:834–836. https://doi.org/10.1038/362834a0.
2. Crowe SA, Jones C, Katsev S, Magen C, O'Neill AH, Sturm A, Canfield DE, Haffner GD, Mucci A, Sundby B, Fowle DA. 2008. Photoferrotrophs thrive in an Archean Ocean analogue. Proc Natl Acad Sci U S A 105:15938–15943. https://doi.org/10.1073/pnas.0805313105.
3. Llirós M, García-Armisen T, Darchambeau F, Morana C, Triadó-Margarit X, Inceoğlu Ö, Borrego CM, Bouillon S, Servais P, Borges AV, Descy JP, Canfield DE, Crowe SA. 2015. Pelagic photoferrotrophy and iron cycling in a modern ferruginous basin. Sci Rep 5:13803. https://doi.org/10.1038/srep13803.
4. Otte JM, Harter J, Laufer K, Blackwell N, Straub D, Kappler A, Kleindienst S. 2018. The distribution of active iron-cycling bacteria in marine and freshwater sediments is decoupled from geochemical gradients. Environ Microbiol 20:2483–2499. https://doi.org/10.1111/1462-2920.14260.
5. Bryce C, Blackwell N, Schmidt C, Otte J, Huang YM, Kleindienst S, Tomaszewski E, Schad M, Warter V, Peng C, Byrne JM, Kappler A. 2018. Microbial anaerobic Fe(II) oxidation—ecology, mechanisms and environmental implications. Environ Microbiol 20:3462–3483. https://doi.org/10.1111/1462-2920.14328.
6. Jiao Y, Newman DK. 2007. The *pio* operon is essential for phototrophic Fe(II) oxidation in *Rhodopseudomonas palustris* TIE-1. J Bacteriol 189:1765–1773. https://doi.org/10.1128/JB.00776-06.
7. Byrne JM, Klueglein N, Pearce C, Rosso KM, Appel E, Kappler A. 2015. Redox cycling of Fe(II) and Fe(III) in magnetite by Fe-metabolizing bacteria. Science 347:1473–1476. https://doi.org/10.1126/science.aaa4834.
8. Olson JM, Blankenship RE. 2004. Thinking about the evolution of photosynthesis. Photosynth Res 80:373–386. https://doi.org/10.1023/B:PRES.0000030457.06495.83.
9. Canfield DE, Rosing MT, Bjerrum C. 2006. Early anaerobic metabolisms. Philos Trans R Soc Lond B Biol Sci 361:1819–1834. https://doi.org/10.1098/rstb.2006.1906.
10. Ehrenreich A, Widdel F. 1994. Anaerobic oxidation of ferrous iron by purple bacteria, a new type of phototrophic metabolism. Appl Environ Microbiol 60:4517–4526.
11. Pierson B, Parenteau M, Griffin B. 1999. Phototrophs in high-iron-concentration microbial mats: physiological ecology of phototrophs in an iron-depositing hot spring. Appl Environ Microbiol 65:5474–5483.
12. Konhauser KO, Hamade T, Raiswell R, Morris RC, Ferris FG, Southam G, Canfield DE. 2002. Could bacteria have formed the Precambrian banded iron formations? Geol 30:1079–1082. https://doi.org/10.1130/0091-7613(2002)030<1079:CBHftp>2.0.CO;2.
13. Kappler A, Newman DK. 2004. Formation of Fe(III)-minerals by Fe(II)-oxidizing photoautotrophic bacteria. Geochim Cosmochim Acta 68:1217–1226. https://doi.org/10.1016/j.gca.2003.09.006.
14. Guzman MS, Rengasamy K, Binkley MM, Jones C, Ranaivoarisoa TO, Singh R, Fike DA, Meacham JM, Bose A. 2019. Phototrophic extracellular electron uptake is linked to carbon dioxide fixation in the bacterium *Rhodopseudomonas palustris*. Nat Commun 10:1355. https://doi.org/10.1038/s41467-019-09377-6.
15. Bose A, Gardel EJ, Vidoudez C, Parra EA, Girguis PR. 2014. Electron uptake by iron-oxidizing phototrophic bacteria. Nat Commun 5:3391. https://doi.org/10.1038/ncomms4391.
16. Rabaey K, Rozendal RA. 2010. Microbial electrosynthesis—revisiting the electrical route for microbial production. Nat Rev Microbiol 8:706–716. https://doi.org/10.1038/nrmicro2422.
17. Lovley DR, Nevin KP. 2013. Electrobiocommodities: powering microbial production of fuels and commodity chemicals from carbon dioxide with electricity. Curr Opin Biotechnol 24:385–390. https://doi.org/10.1016/j.copbio.2013.02.012.
18. Tefft NM, TerAvest MA. 2019. Reversing an extracellular electron transfer pathway for electrode-driven acetoin reduction. ACS Synth Biol 8:1590–1600. https://doi.org/10.1021/acssynbio.8b00498.
19. Shi L, Squier TC, Zachara JM, Fredrickson JK. 2007. Respiration of metal (hydr)oxides by Shewanella and Geobacter: a key role for multihaem c-type cytochromes. Mol Microbiol 65:12–20. https://doi.org/10.1111/j.1365-2958.2007.05783.x.
20. Albers SV, Meyer BH. 2011. The archaeal cell envelope. Nat Rev Microbiol 9:414–426. https://doi.org/10.1038/nrmicro2576.
21. Hartshorne RS, Reardon CL, Ross D, Nuester J, Clarke TA, Gates AJ, Mills PC, Fredrickson JK, Zachara JM, Shi L, Beliaev AS, Marshall MJ, Tien M, Brantley S, Butt JN, Richardson DJ. 2009. Characterization of an electron conduit between bacteria and the extracellular environment. Proc Natl Acad Sci U S A 106:22169–22174. https://doi.org/10.1073/pnas.0900086106.
22. Coursolle D, Gralnick JA. 2010. Modularity of the Mtr respiratory pathway of *Shewanella oneidensis* strain MR-1. Mol Microbiol 77:995–1008. https://doi.org/10.1111/j.1365-2958.2010.07266.x.
23. Coursolle D, Baron DB, Bond DR, Gralnick JA. 2010. The Mtr respiratory pathway is essential for reducing flavins and electrodes in *Shewanella oneidensis*. J Bacteriol 192:467–474. https://doi.org/10.1128/JB.00925-09.
24. Bretschger O, Obraztsova A, Sturm CA, Chang IS, Gorby YA, Reed SB, Culley DE, Reardon CL, Barua S, Romine MF, Zhou J, Beliaev AS, Bouhenni R, Saffarini D, Mansfeld F, Kim BH, Fredrickson JK, Nealson KH. 2007. Current production and metal oxide reduction by *Shewanella oneidensis* MR-1 wild type and mutants. Appl Environ Microbiol 73:7003–7012. https://doi.org/10.1128/AEM.01087-07.
25. Rowe AR, Rajeev P, Jain A, Pirbadian S, Okamoto A, Gralnick JA, El-Naggar MY, Nealson KH. 2018. Tracking electron uptake from a cathode into *Shewanella* cells: implications for energy acquisition from solid-substrate electron donors. mBio 9:e02203-17. https://doi.org/10.1128/mBio.02203-17.
26. Appia-Ayme C, Guiliani N, Ratouchniak J, Bonnefoy V. 1999. Characterization of an operon encoding two *c*-type cytochromes, an *aa3*-type

cytochrome oxidase, and rusticyanin in Thiobacillus ferrooxidans ATCC 33020. Appl Environ Microbiol 65:4781–4787.
27. Blake R, Shute EA, Waskovsky J, Harrison AP. 1992. Respiratory components in acidophilic bacteria that respire on iron. Geomicrobiol J 10: 173–192. https://doi.org/10.1080/01490459209377919.
28. Yamanaka T, Fukumori Y. 1995. Molecular aspects of the electron transfer system which participates in the oxidation of ferrous ion by Thiobacillus ferrooxidans. FEMS Microbiol Rev 17:401–413. https://doi.org/10.1111/j.1574-6976.1995.tb00222.x.
29. Croal LR, Jiao Y, Newman DK. 2007. The fox operon from *Rhodobacter* strain SW2 promotes phototrophic Fe(II) oxidation in *Rhodobacter capsulatus* SB1003. J Bacteriol 189:1774–1782. https://doi.org/10.1128/JB.01395-06.
30. Yarzábal A, Brasseur G, Ratouchniak J, Lund K, Lemesle-Meunier D, DeMoss JA, Bonnefoy V. 2002. The high-molecular-weight cytochrome *c* Cyc2 of *Acidithiobacillus ferrooxidans* is an outer membrane protein. J Bacteriol 184:313–317. https://doi.org/10.1128/jb.184.1.313-317.2002.
31. Liu J, Wang Z, Belchik SM, Edwards MJ, Liu C, Kennedy DW, Merkley ED, Lipton MS, Butt JN, Richardson DJ, Zachara JM, Fredrickson JK, Rosso KM, Shi L. 2012. Identification and characterization of MtoA: a decaheme c-type cytochrome of the neutrophilic Fe(II)-oxidizing bacterium *Sideroxydans lithotrophicus* ES-1. Front Microbiol 3:37. https://doi.org/10.3389/fmicb.2012.00037.
32. Jiao Y, Kappler A, Croal LR, Newman DK. 2005. Isolation and characterization of a genetically tractable photoautotrophic Fe(II)-oxidizing bacterium, *Rhodopseudomonas palustris* strain TIE-1. Appl Environ Microbiol 71:4487–4496. https://doi.org/10.1128/AEM.71.8.4487-4496.2005.
33. Bird LJ, Bonnefoy V, Newman DK. 2011. Bioenergetic challenges of microbial iron metabolisms. Trends Microbiol 19:330–340. https://doi.org/10.1016/j.tim.2011.05.001.
34. Bird LJ, Saraiva IH, Park S, Calçada EO, Salgueiro CA, Nitschke W, Louro RO, Newman DK. 2014. Nonredundant roles for cytochrome c2 and two high-potential iron-sulfur proteins in the photoferrotroph *Rhodopseudomonas palustris* TIE-1. J Bacteriol 196:850–858. https://doi.org/10.1128/JB.00843-13.
35. Bose A, Newman DK. 2011. Regulation of the phototrophic iron oxidation (*pio*) genes in *Rhodopseudomonas palustris* TIE-1 is mediated by the global regulator, FixK. Mol Microbiol 79:63–75. https://doi.org/10.1111/j.1365-2958.2010.07430.x.
36. Feissner RE, Richard-Fogal CL, Frawley ER, Loughman JA, Earley KW, Kranz RG. 2006. Recombinant cytochromes *c* biogenesis systems I and II and analysis of haem delivery pathways in *Escherichia coli*. Mol Microbiol 60:563–577. https://doi.org/10.1111/j.1365-2958.2006.05132.x.
37. Feissner R, Xiang Y, Kranz RG. 2003. Chemiluminescent-based methods to detect subpicomole levels of c-type cytochromes. Anal Biochem 315:90–94. https://doi.org/10.1016/s0003-2697(02)00658-9.
38. Hancock R, Carey AM. 1979. Outer membrane of *Pseudomonas aeruginosa*: heat-2-mercaptoethanol-modifiable proteins. J Bacteriol 140: 902–910.
39. Beher MG, Schnaitman CA, Pugsley AP. 1980. Major heat-modifiable outer membrane protein in gram-negative bacteria: comparison with the ompA protein of *Escherichia coli*. J Bacteriol 143:906–913.
40. Poolman J, De Marie S, Zanen H. 1980. Variability of low-molecular-weight, heat-modifiable outer membrane proteins of *Neisseria meningitidis*. Infect Immun 30:642–648.
41. Kent NE, Wisnieski BJ. 1983. Heat modifiability and detergent solubility of outer-membrane proteins of *Rhodopseudomonas sphaeroides*. J Bacteriol 156:956–961.
42. Noinaj N, Kuszak AJ, Buchanan SK. 2015. Heat modifiability of outer membrane proteins from Gram-negative bacteria. Methods Mol Biol 1329:51–56. https://doi.org/10.1007/978-1-4939-2871-2_4.
43. Bagos PG, Nikolaou EP, Liakopoulos TD, Tsirigos KD. 2010. Combined prediction of Tat and Sec signal peptides with hidden Markov models. Bioinformatics 26:2811–2817. https://doi.org/10.1093/bioinformatics/btq530.
44. Katzke N, Arvani S, Bergmann R, Circolone F, Markert A, Svensson V, Jaeger KE, Heck A, Drepper T. 2010. A novel T7 RNA polymerase dependent expression system for high-level protein production in the phototrophic bacterium *Rhodobacter capsulatus*. Protein Expr Purif 69: 137–146. https://doi.org/10.1016/j.pep.2009.08.008.
45. Berry EA, Trumpower BL. 1987. Simultaneous determination of hemes a, b, and c from pyridine hemochrome spectra. Anal Biochem 161:1–15. https://doi.org/10.1016/0003-2697(87)90643-9.
46. Sutherland MC, Tran NL, Tillman DE, Jarodsky JM, Yuan J, Kranz RG. 2018. Structure-function analysis of the bifunctional CcsBA heme exporter and cytochrome *c* synthetase. mBio 9:e02134-18. https://doi.org/10.1128/mBio.02134-18.
47. Schicklberger M, Bücking C, Schuetz B, Heide H, Gescher J. 2011. Involvement of the *Shewanella oneidensis* decaheme cytochrome MtrA in the periplasmic stability of the *β*-barrel protein MtrB. Appl Environ Microbiol 77:1520–1523. https://doi.org/10.1128/AEM.01201-10.
48. Lovley DR. 2008. Extracellular electron transfer: wires, capacitors, iron lungs, and more. Geobiology 6:225–231. https://doi.org/10.1111/j.1472-4669.2008.00148.x.
49. Rosenbaum MA, Bar HY, Beg QK, Segrè D, Booth J, Cotta MA, Angenent LT. 2011. *Shewanella oneidensis* in a lactate-fed pure-culture and a glucose-fed co-culture with *Lactococcus lactis* with an electrode as electron acceptor. Bioresour Technol 102:2623–2628. https://doi.org/10.1016/j.biortech.2010.10.033.
50. Deutzmann JS, Sahin M, Spormann AM. 2015. Extracellular enzymes facilitate electron uptake in biocorrosion and bioelectrosynthesis. mBio 6:e00496-15. https://doi.org/10.1128/mBio.00496-15.
51. Rengasamy K, Ranaivoarisoa T, Singh R, Bose A. 2018. An insoluble iron complex coated cathode enhances direct electron uptake by *Rhodopseudomonas palustris* TIE-1. Bioelectrochemistry 122:164–173. https://doi.org/10.1016/j.bioelechem.2018.03.015.
52. Heising S, Schink B. 1998. Phototrophic oxidation of ferrous iron by a *Rhodomicrobium vannielii* strain. Microbiology 144:2263–2269. https://doi.org/10.1099/00221287-144-8-2263.
53. Duchow E, Douglas H. 1949. *Rhodomicrobium vannielii*, a new photoheterotrophic bacterium. J Bacteriol 58:409–416.
54. Tushar L, Sasikala C, Ramana CV. 2014. Draft genome sequence of *Rhodomicrobium udaipurense* JA643T with special reference to hopanoid biosynthesis. DNA Res 21:639–647. https://doi.org/10.1093/dnares/dsu026.
55. Källberg M, Wang H, Wang S, Peng J, Wang Z, Lu H, Xu J. 2012. Template-based protein structure modeling using the RaptorX web server. Nat Protoc 7:1511–1522. https://doi.org/10.1038/nprot.2012.085.
56. Danese PN, Silhavy TJ. 1998. Targeting and assembly of periplasmic and outer-membrane proteins in *Escherichia coli*. Annu Rev Genet 32:59–94. https://doi.org/10.1146/annurev.genet.32.1.59.
57. White GF, Shi Z, Shi L, Wang Z, Dohnalkova AC, Marshall MJ, Fredrickson JK, Zachara JM, Butt JN, Richardson DJ, Clarke TA. 2013. Rapid electron exchange between surface-exposed bacterial cytochromes and Fe(III) minerals. Proc Natl Acad Sci U S A 110:6346–6351. https://doi.org/10.1073/pnas.1220074110.
58. San Francisco B, Bretsnyder EC, Rodgers KR, Kranz RG. 2011. Heme ligand identification and redox properties of the cytochrome c synthetase, CcmF. Biochemistry 50:10974–10985. https://doi.org/10.1021/bi201508t.
59. San Francisco B, Sutherland MC, Kranz RG. 2014. The CcmFH complex is the system I holocytochrome c synthetase: engineering cytochrome c maturation independent of CcmABCDE. Mol Microbiol 91:996–1008. https://doi.org/10.1111/mmi.12510.
60. Shi L, Dong H, Reguera G, Beyenal H, Lu A, Liu J, Yu HQ, Fredrickson JK. 2016. Extracellular electron transfer mechanisms between microorganisms and minerals. Nat Rev Microbiol 14:651–662. https://doi.org/10.1038/nrmicro.2016.93.
61. Sutherland MC, Rankin JA, Kranz RG. 2016. Heme trafficking and modifications during system I cytochrome c biogenesis: insights from heme redox potentials of Ccm proteins. Biochemistry 55:3150–3156. https://doi.org/10.1021/acs.biochem.6b00427.
62. Croal LR, Johnson CM, Beard BL, Newman DK. 2004. Iron isotope fractionation by Fe(II)-oxidizing photoautotrophic bacteria. Geochim Cosmochim Acta 68:1227–1242. https://doi.org/10.1016/j.gca.2003.09.011.
63. Stookey LL. 1970. Ferrozine—a new spectrophotometric reagent for iron. Anal Chem 42:779–781. https://doi.org/10.1021/ac60289a016.